ELSEVIER

Journal of Alloys and Compounds 228 (1995) 49–53

Journal of ALLOYS AND COMPOUNDS

The magnetic properties of HoNiBC: absence of superconductivity and helical ground-state

M. El Massalami[a], E. Baggio-Saitovitch[a], A. Sulpice[b]

[a]*CBPF, R.X. Sigaud 150, CEP 22290-180, Rio de Janeiro, Brazil*
[b]*CNRS, CRTBT, BP166, 38042 Grenoble, Cedex 9, France*

Received 24 February 1995

Abstract

The magnetic and transport properties of the quaternary intermetallic HoNiBC compound (space group $P4/nmm$, $a = 3.563(1)$ Å, $c = 7.546(1)$ Å) were studied for 1.2 K $\leq T \leq$ 300 K and $H \leq 80$ kOe. The compound orders antiferromagnetically at 9.8(3) K and, in the ordered state, the Ho moment saturates to 8.5(1) μ_B. In contrast with the structurally-related reentrant superconductor $HoNi_2B_2C$, superconductivity is not found nor are there indications of a helical ground-state in the whole temperature range. These features are attributed, respectively, to the positioning of the Fermi level at a DOS minimum and the presence of the HoC double layers that inhibits the establishment of a helical spin arrangement.

Keywords: Intermetallic boro-carbide; HoNiBC; Antiferromagnetism

1. Introduction

Recently, two families of the nickel boro-carbide series $(RC)_n(Ni_2B_2)$ were discovered [1,2]. The crystal structure of the much studied RNi_2B_2C family ($n = 1$) is a filled variant on the $ThCr_2Si_2$ structure [3,4]. It is a body-centered tetragonal structure (space group $I4/mmm$) where RC layers are alternately stacked on the Ni_2B_2 layers in the following sequences $(RC\text{-}B\text{-}Ni_2\text{-}B)_m$ (Fig. 1(a)). On the other hand, the structure of LuNiBC, as a representative of the less studied RNiBC family ($n = 2$), adopts a simple tetragonal structure (space group $P4/nmm$) [3,4]. In contrast to the layer stacking in the RNi_2B_2C family, the RC sheets are paired as double NaCl-type layers that are spatially separated by the Ni_2B_2 blocks resulting in the sequences $(RC\text{-}RC\text{-}B\text{-}Ni_2\text{-}B)_m$ (Fig. 1(b)).

It is interesting to see whether the above mentioned structural–chemical similarities of the two families are translated into similarity of the physical properties. On the one hand, the only studied member of the RNiBC series is LuNiBC [3,4]. It is a metallic nonsuperconductor where the absence of superconductivity is shown, by electronic structure calculation, to be due to the positioning of the Fermi level at a density of state (DOS) minimum [5]. However, the magnetic and the

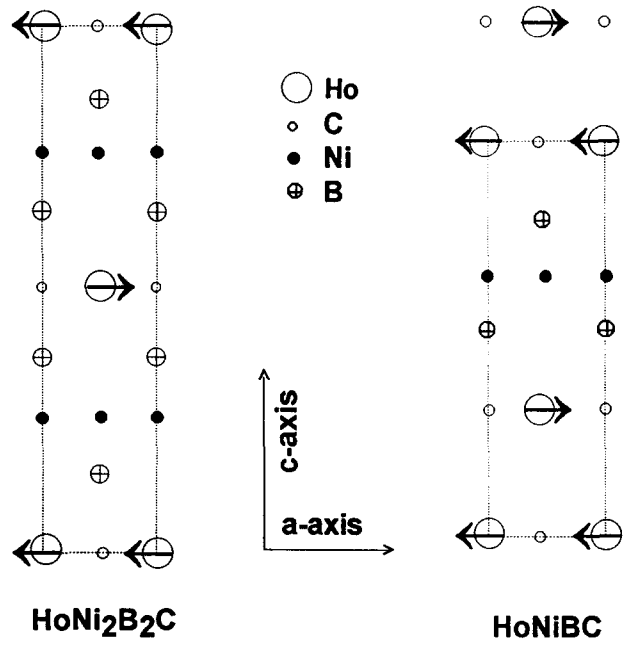

Fig. 1. The *ac*-plane projection of the structural features and the magnetic ground state at $T = 0$ K of $HoNi_2B_2C$ and HoNiBC. The units cells are marked by dotted lines. The arrows indicate the orientations of the Ho moments.

Elsevier Science S.A.
SSDI 0925-8388(95)01669-4

superconducting properties of the RNi_2B_2C family show quite interesting features [2,6–16]. As an example, the competition between superconductivity and magnetism in the R = Tm, Er, Ho, Dy, Tb, Gd compounds classify the series into the following different groups: superconducting antiferromagnets (R = Tm, Er, Ho ($T < 4$ K)), reentrant superconductor (Ho) and normal anti-ferromagnets ($4 < T < 5$ K) Tb, (R = Dy, Gd). In particular, the origin of the reentrant behavior in $HoNi_2B_2C$ [6,8,9,11,12,13] is related to the presence of the helical ground-state.

Our aim in this work is to study the magnetic and transport features of HoNiBC and to compare these properties with those of $HoNi_2B_2C$. In Section 3, after asserting its structural character, we show that it is a nonsuperconducting AFM metal. In Section 4 we associate the absence of the superconductivity and the helical ground-state in HoNiBC with its specific structural–chemical character.

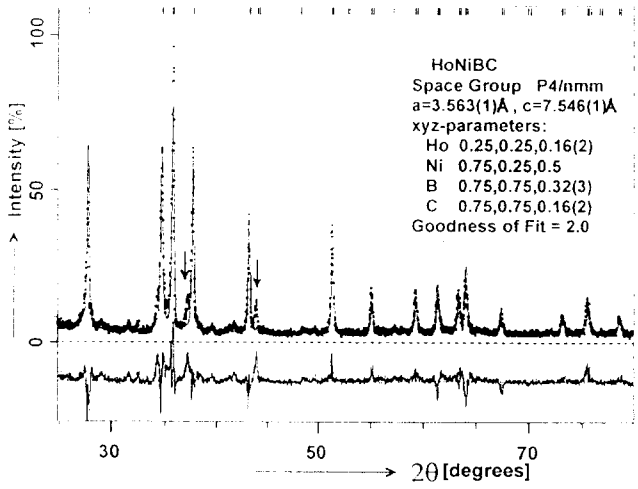

Fig. 2. The CuKα diffractogram of HoNiBC. The mid-field shows the experimental points (dots) and the theoretical fit (continuous line). The Bragg lines are shown at the top field (short vertical bar) while the difference (continuous line) is shown in the lower field. The most strong peaks of the impurity phases are denoted by two short vertical arrows. The text inset gives some of the obtained structural parameters.

2. Experimental

A conventional argon arc-melt method was used for sample preparation [2]. The as-prepared sample was wrapped in Ta foil and vacuum-annealed for two days at 900 °C. After annealing, the button was quenched in liquid nitrogen. Standard powder CuKα X-ray diffraction at ambient temperatures together with the Rietveld refinement analysis were used for structural characterization. The magnetization was measured on a commercial SQUID magnetometer. The a.c. susceptometer was driven by a 1 Oe sinusoidal field oscillating at 500 Hz. The d.c. resistivity was measured in a four point geometry. The longitudinal magnetoresistivity ($j//H$) was measured in fields up to 80 kOe using the four-point d.c. resistivity method. The sample temperature was monitored by carbon glass thermometer with its long axis set perpendicular to the field direction. Temperatures were corrected for magnetic field influence following the procedure described in Ref. [17].

3. Results

For the structural analysis of X-ray diffractogram (Fig. 2) we assumed the same structural model which was proposed for LuNiBC [3,4]: a tetragonal system with a space group $P4/nmm$. In fact, the atomic position, occupation and thermal parameters of LuNiBC [3,4] were taken as the starting parameters for our Rietveld refinement procedures. The numerical convergence of the profile fit was limited only by the presence of unidentified impurity phases. The results of the refinement are shown in Fig. 2, the strongest lines due to impurities being denoted by short vertical arrows. The presence of considerable preferred orientation features is attributed to the misrepresentative aspect within the powdered sample resulting from preferred cleavage along the basal plane.

In Refs. [3] and [4] it was shown that the width of the B-Ni_2-B layers (and thus the separating distance between the RC sheets) as well as most of the chemical bonding lengths in both of LuNiBC and $LuNi_2B_2C$ are almost equal. We found the same results when comparing the structural features of HoNiBC and $HoNi_2B_2C$.

Magnetic susceptibility measurements (Fig. 3) show a Curie–Weiss (CW) behavior down to ca. 17 K. The effective moment is found to be 11.3(1) μ_B, which is 9% higher than the theoretically expected value for Ho^{3+} ion (10.4 μ_B). In addition, Fig. 3 shows that the paramagnetic characteristic temperature (θ) is 9.6(1) K while the long range antiferromagnetic (AFM) order sets in at $T_N = 9.8(3)$ K. Such a closeness between T_N and $\theta\left(\frac{T_N}{\theta} = 1.02\right)$ reflects a stronger three-dimensional magnetic character as compared to the one observed in $HoNi_2B_2C$ $\left(\frac{T_N}{\theta} = 3.85\right)$ [6,9]. Moreover, the Néel temperature for HoNiBC is almost twice that of $HoNi_2B_2C$ (Table 1). Naturally, these features are connected with the increased number of the magnetic layers in the former compound. Fig. 3 shows, in addition, two features that deserve some comment[1].

[1] We are indebted to the referee for suggesting an interpretation for these two features.

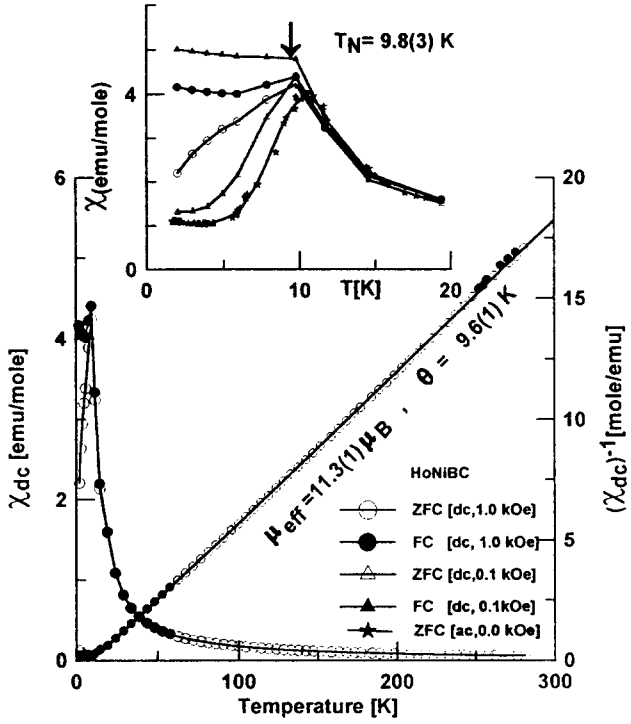

Fig. 3. Field-cooled (FC) and zero-field-cooled (ZFC) magnetic susceptibilities of HoNiBC. The inset shows the a.c. susceptibility at zero field (stars) as well as the FC (filled circles and triangles) and ZFC (empty circles and triangles) d.c. susceptibilities at different fields.

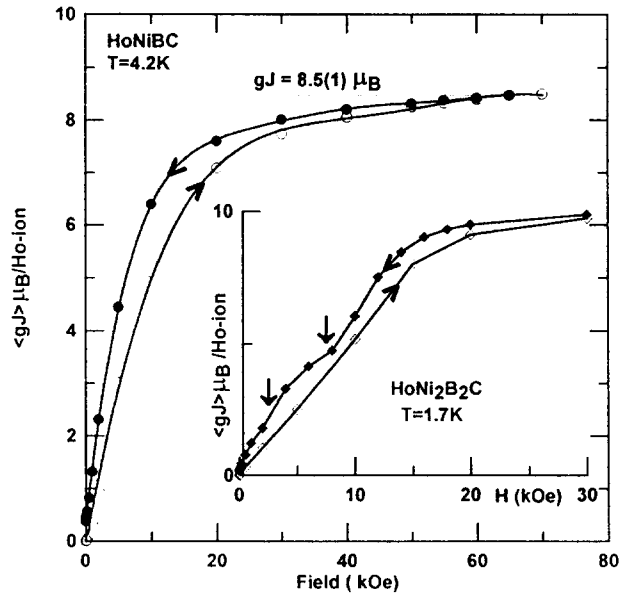

Fig. 4. The magnetization isotherm at $T = 2$ K of HoNiBC. The inset shows the magnetization isotherm for $HoNi_2B_2C$ at 1.7 K wherein the two intermediate field-induced phase transitions are denoted by vertical arrows [14].

First, for $T < T_N$ considerable differences exist between field-cooled and zero-field cooled measurements (see the inset of Fig. 3). This effect may be attributed to the presence of a small amount (few %) of atomic disorder (such as C-deficiency or B–C site interchange) that are beyond XRD diffraction resolution. Second, the deviation from the CW-law starts well above T_N. This is most likely due to short range ordering. Fig. 3 shows the absence of superconductivity in the whole measured temperature range.

The magnetization isotherm at $T = 2$ K (Fig. 4) shows a smooth monotonic rise with the applied field up to 30 kOe, above which it shows a slow quasi-linear rise. The extrapolated saturation moment per Ho ion is 8.5(1) μ_B. This value is 15% lower than the expected moment for ionic Ho^{3+} and 6% lower than the corresponding saturation moment of $HoNi_2B_2C$ [9] (see Table 1). Since the *4mm* point symmetry at the Ho site in HoNiBC is lower than *4/mmm* at the corresponding site in $HoNi_2B_2C$, it is tempting to attribute this lowering of the saturation moment to the influence of a stronger crystalline electric field.

No attempts were made to analyze the results of Fig. 4 for spin-flop field or anisotropic forces because of the polycrystalline form of the sample. For comparison, we include the powder magnetization isotherm of $HoNi_2B_2C$ [14] as an inset in Fig. 4. It is evident that the moment saturation in HoNiBC is harder to achieve than in $HoNi_2B_2C$, indicating stronger anisotropic forces. Furthermore, the inset of Fig. 4 shows that on saturating the magnetic moment of the polycrystalline $HoNi_2B_2C$ and ramping down the field, the helical spin structure is revealed as a step-like structure in the M–H curve [9,14]. Therefore, the absence of any step-like structure in the magnetization isotherms of HoNiBC (Fig. 4) and the smooth behavior of the susceptibility below T_N (see the inset in Fig. 3) suggest that there is no helical spin arrangement in this compound.

DC resistivity (Fig. 5) shows a conventional metallic behavior at high temperatures and, as evident, there are no traces of superconductivity down to 1.2 K. The longitudinal magnetoresistivity ($j//H$) is shown in the

Table 1
Comparison of some of the structural and magnetic properties of HoNiBC and $HoNi_2B_2C$[a]

Compound	Space group	Ho-site symmetry	a (Å)	c (Å)	μ μ_B	T_N (K)	θ (K)
HoNiBC	*P4/nmm*	*4mm*	3.563(1)	7.546(1)	8.5(1)	9.8(3)	9.6(1)
$HoNi_2B_2C$	*I4/mmm*	*4/mmm*	3.520(1)	10.521(1)	9.0	5.0	1.3

[a] The magnetic data of $HoNi_2B_2C$ are taken from Refs. [6] and [9].

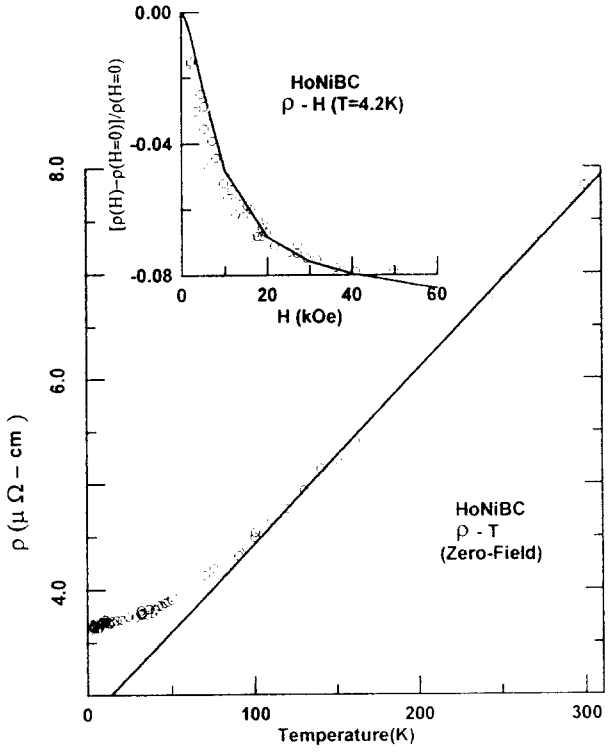

Fig. 5. The d.c. resistivity in zero-field of HoNiBC. Inset: the longitudinal ($j//H$) magnetoresistivity is shown as $\rho\ (H) - \rho(H = 0)]/\rho\ (H = 0)$ vs. H without subtracting the nonmagnetic contribution to the resistivity. The solid line in the insert shows the scaling to $\langle gJ \rangle^2$ (see text).

inset of Fig. 5. $\Delta\rho(H)/\rho(H = 0) = [\rho(H) - \rho(H = 0)]/\rho(H = 0))$ shows that the magnetic contribution to the resistivity decreases monotonically with H. Mean field approximation relates $\Delta\rho(H)/\rho(H = 0)$ to the thermally averaged Ho moment $\langle gJ \rangle$ along the field direction by the following relation [18]:

$$\Delta\rho(H)/\rho(H = 0) \propto \langle gJ \rangle^2 \quad (1)$$

It is expected that the $\langle$gJ$\rangle$ vs. H curve at $T = 2$ K (Fig. 4) will be similar to the curve at $T = 4.2$ K. The experimentally determined $\langle$gJ$\rangle$in Fig. 4 can therefore be substituted into Eq. (1) and can be compared to the measured $\Delta\rho(H)/\rho(H = 0)$. This is shown in the inset of Fig. 5 where the solid line is the scaling of $\langle gJ \rangle^2$ to $\Delta\rho(H)/\rho(H = 0)$ values. It may be worth recalling that, first, the sample is a textured polycrystal and is contaminated with a minority of impurity phases and second, no correction is made to account for the contribution of the lattice and the temperature-independent resistivities. Nevertheless, it may be seen that the inset of Fig. 5 shows qualitative agreement with the prediction of Eq. (1) in fields up to 60 kOe.

4. Discussion

It was shown in Section 3 that although HoNiBC and $HoNi_2B_2C$ are structurally related, their physical behaviors are distinctly different. We discuss below two characteristic differences: the absence of superconductivity and helical spin arrangement.

Based on the structural isomorphism between LuNiBC and HoNiBC and assuming the validity of the rigid-band model [18], we would expect their electronic band structures to be similar. As with the case of LuNiBC, therefore, the absence of superconductivity in HoNiBC indicates that the Fermi level is still at a DOS minimum. In other words, the replacement of the Lu ion by the Ho ion does not influence drastically the position of the Fermi level even though the substitutent has a larger ionic size and may contribute differently to the formation of the conduction band. For the discussion of the magnetic properties, let us assume that the dominant RKKY-type interactions can be described as follows: ferromagnetic (FM) couplings within the planes and AFM couplings among the neighboring and nearest-neighboring planes. The observation that θ is positive gives an indication of dominant FM interactions (even though AFM interactions are responsible for the long-range three-dimensional order). For instance, the in-plane FM interactions might be much stronger than the inter-planar AFM interactions.

From considerations of energy cost minimization, it is expected that the specific structural arrangement of the HoC layers will exclude, at $T = 0$, the helical spin state in favor of the AFM arrangement as shown in Fig. 1(b). A helical state will be expected only if the AFM-coupled layers are evenly spaced along the spiral axis [18]. This is the case with $HoNi_2B_2C$ [7,13] wherein the AFM coupled HoC layers are evenly spaced along the c-axis making it possible to sustain a constant spiral angle between the moment orientations of adjacent FM sheets.

5. Conclusion

The insertion of additional HoC layers in the structure of $HoNi_2B_2C$ leads to drastic changes in the physical properties of the resulting HoNiBC compound. The Fermi level is shifted to a DOS minimum (thus there is no superconductivity). The average strength of the magnetic couplings is enhanced as reflected in higher values of the ordering temperature and the saturation field. Furthermore, the resulting uneven spacing of the HoC layers seems to destabilize the helical state in favor of a simple AFM state.

Acknowledgment

R. Pereira is thanked for taking the XRD diffractogram.

References

[1] R. Nagarajan, C. Mazumdar, Z. Hossein, S.K. Dhar, K.V. Golpakrishna, L.C. Gupta, C. Godart, B.D. Padalia and R. Vijayaragharan, *Phys. Rev. Lett., 72* (1994) 274.

[2] R.J. Cava, H. Takagi, B. Batlogg, H.W. Zandbergrn, J.J. Krajewski, W.F. Peck, Jr, T. Siegrist, B. Batlog, R.B. van Dover, R.J. Felder, K. Mizuhashi, J.O. Lee, H. Eisaki and S. Uchida, *Nature, 367* (1994) 252.

[3] T. Siegrist, H.W. Zandbergen, R.J. Cava, J.J. Krajewski and W.F. Peck, *Nature, 367* (1994) 252.

[4] H.W. Zandbergen, R.J. Cava, J.J. Krajewski, W.F. Peck, Jr., *Physica, C224* (1994) 6.

[5] L.F. Mattheiss, *Phys. Rev. B49* (1994) 13279.

[6] H. Eisaki, T. Takagi, R.C. Cava, K. Mizuhashi, J.O. Lee, B. Batlogg, J.J. Krajewski, W.F. Peck and S. Uchida, *Phys. Rev., B50* (1994) 647.

[7] T.E. Grigereit, J.W. Lynn, Q. Huang, A. Santoro, R.J. Cava, J.J. Krajewski and W.F. Peck, Jr, *Phys. Rev. Let. 73* (1994) 2756; Q. Huang, A. Santoro, T.E. Grigereit, J.W. Lynn, R.C. Cava, J.J. Krajewski and W.F. Peck, *Phys. Rev., B51* (1995) in press.

[8] R. Movshovich, M.F. Hundley, J.D. Thompson, P.C. Canfield, B.K. Cho and A.V. Chubukov, *Physica, C227* (1994) 381.

[9] P.C. Canfield, B. K Cho, D.C. Johnston, D.K. Finemore and M.F. Hundley, *Physica, C230* (1994) 397.

[10] M. El Massalami, S.L. Bud'ko, B. Giordanengo and E.M. Baggio-Saitovitch, *Physica C, 244* (1995).

[11] S.K. Sinha, J.W. Lynn, T.E. Griegereit, Z. Hossain, L.C. Gupta, R. Nagarajan and C. Godart, *Phys. Rev., B51* (1995), in press.

[12] H. Schmidt and H.F. Braun, *Physica C, 229* (1994) 315.

[13] A.I. Goldman, C. Stassis, P.C. Canfield, J. Zarestky, P. Dervenagas, B.K. Cho and D.C. Johnston, *Phys. Rev., B50* (1995) 9668.

[14] M. El Massalami et al, *J. Magn. Magn. Mater.*, in press.

[15] M. El Massalami, S.L. Bud'ko, B. Giordanengo, M.B. Fontes, J.C. Mondragon and E.M. Baggio-Saitovitch, *Physica, C235–240* (1994) 2563; M. El Massalami, S.L. Bud'ko, B. Giordanengo, M.B. Fontes, J.C. Mondragon and E.M. Baggio-Saitovitch, *Physica Status Solidi (b)*, in press.

[16] M. El Massalami, B. Giordanengo, E.M. Baggio-Saitovitch, J. Voirn and A. Sulpice, *J. Phys.: Condens. Matter*, in press.

[17] H.H. Sample, B.L. Brandt and L.G. Rubin, *Rev. Sci. Instrum. 53* (1982) 1129.

[18] B. Coqblin, *The Electronic Structure of Rare-Earth Metaland Alloys: the Magnetic Heavy Rare-Earth,* Academic Press, London, 1977. [19] S.V. Vonsovsky, Yu.A. Izyumov and E.Z. Kurmaev, *Superconducitivity of Transition Metals,* Springer Series in Solid-state Sciences 27, New York, 1982.